Feedback Control Based Active Cooling With Pre-estimated Reliability For Stabilizing The Thermal Error of a Precision Mechanical Spindle

Mohan Lei (salingerr@outlook.com)
Xi'an University of Technology
Feng Gao
Xi'an University of Technology
Yan Li
Xi'an University of Technology
Ping Xia
Xi'an Jiaotong University
Mengchao Wang
Xi'an Jiaotong University
Jun Yang
Xi'an Jiaotong University

Research Article

Keywords: Precision mechanical spindle, Active cooling, Thermal error feedback control, Thermal error stabilization, Thermal equilibrium

Posted Date: November 1st, 2021

DOI: https://doi.org/10.21203/rs.3.rs-1018070/v1

Feedback control based active cooling with pre-estimated reliability for stabilizing the thermal error of a precision mechanical spindle

*Mohan Lei[1, 2], Feng Gao[1, 2], Yan Li[1, 2], Ping Xia[3], Mengchao Wang[3], Jun Yang[3]

[1] *Key Lab of Manufacturing Equipment of Shaanxi Province, School of Mechanical and Precision Instrument Engineering, Xi'an University of Technology, Xi'an 710048, China*

[2] *Key Lab of NC Machine Tools and Integrated Manufacturing Equipment of the Ministry of Education, Xi'an University of Technology, Xi'an 710048, China*

[3] *State Key Laboratory for Manufacturing Systems Engineering, Xi'an Jiaotong University, Xi'an, 710049, Shaanxi, China*

*E-mail: *salingerr@outlook.com*

Abstract

Thermal error stability (STE) of the spindle determines the machining accuracy of a precision machine tool. Here we propose a thermal error feedback control based active cooling strategy for stabilizing the spindle thermal error in long-term. The strategy employs a cooling system as actuator and a thermal error regression model to output feedback. Structural temperature measurements are considerably interfered by the active cooling, so the regression models trained with experimental data might output inaccurate feedbacks in unseen work conditions. Such inaccurate feedbacks are the major cause for excessive fluctuations and failures of the thermal error control processes. Independence of the thermal data is analyzed, and a V-C (Vapnik-Chervonenkis) dimension based approach is presented to estimate the generalization error bound of the regression models. Then, the model which is most likely to give acceptable performance can be selected, the reliability of the feedbacks can be pre-

estimated, and the risk of unsatisfactory control effect will be largely reduced. Experiments under different work conditions are conducted to verify the proposed strategy, the thermal error is stabilized to be within a range smaller than 1.637μm, and thermal equilibrium time is advanced by more than 78.3%.

Keywords: Precision mechanical spindle; Active cooling; Thermal error feedback control; Thermal error stabilization; Thermal equilibrium.

1. Introduction

Thermal error contributes to about 70% of the total machining error in precision machine tools[1-4]. Spindle is one core component of a precision machine tool, thermal error of the spindle is the major factor leads to the deterioration of machining accuracy for machine tools[5-7]. Precision machine tools usually preheats for long period to achieve thermal equilibrium before machining. Then, the relative position between the workpiece coordinate system and the machine coordinate system will be adjusted by tool setting, so that the stable part of the thermal error will be eliminated. We can conclude that the fluctuation range or stability of the spindle thermal error is a dominant factor that affects the machining accuracy.

Active cooling is an effective way to suppress the thermal deformation of a precision spindle. Liu et al. developed a closed-loop bath recirculation system for temperature control of a motorized spindle, the coolant supply power is adjusted to control the temperature rise between the outlet and inlet of the cooling channel, that is the spindle heat dissipation from cooling[8]. A power matching based heat dissipation strategy is then proposed, the coolant temperature varies with the estimated heat generation of the component under cooling[9]. Grama et al. proposed the Cooler Trigger Model strategy for temperature control of a spindle, which dynamically controls the switching frequency of the cooler compressor so that the heat extraction is in accordance with the estimated heat generation rate[10]. Ge et al. presented an external cooling equipment for a spindle, which includes a cooling unit, CFRP (Carbon Fiber Reinforced Polymer) bars, and thermoelectric modules[11]. The external cooling

largely reduced the thermal deformation of the spindle. According to the heat generation estimation of the spindle components, constant coolant temperature cooling experiment for a precision spindle is carried out by our research team[12], the spindle thermal error is significantly reduced, but still not stabilized.

Aforementioned active cooling strategies aim at minimizing the overall deformation of the spindle structure, so that the thermal error can be reduced to minimum. But such strategies are generally performed based on constant coolant temperature or offline empirical and theoretical heat generation models, hence the heat dissipation rate cannot accurately adapt to the rapidly-changing dynamic thermal characteristics of the spindle and the thermal error can hardly be kept stable in long-term. Moreover, strategies aim at dissipating all generated heat and minimize overall structural deformation usually consume large amount of energy and bring extra costs such as complex cooling-channels structure and a multiple-loops cooling system.

Here we propose a thermal error feedback control based active cooling strategy for the mechanical spindle in a precision boring machine. This strategy regards the "spindle-thermal error-active cooling" system as a feedback control system, which employs temperature online measuring and a thermal error model to output feedback in real-time, and uses the cooler as actuator. The thermal error feedback control strategy does not seek to minimize the thermal deformation of the overall spindle structure, but to maintain the long-term stability so the thermal-induced error in machining can be minimized (by tool-setting). As a result, this strategy consumes low energy in the active cooling, and it can be put into practice without raising extra costs of multi-loops cooling system, modifying flow channel structure or additional cooling devices.

Much effort has been made to study high-quality data-driven regression modeling methods for the spindle thermal error, and the modeling methods are widely used in the thermal error compensation for various spindles[6, 13-15]. It seems such regression modeling methods can also be used for the thermal error feedback control, the online-temperature measurements can be used as the inputs for the spindle thermal error regression model, and the model can output feedback in real-time for the thermal error feedback control. Then, the coolant temperature will be adjusted according to the

difference between the estimated thermal error and the RITE (Reference Input of Thermal Error).

However, as we have observed in experiments, the recirculation of the temperature-varying coolant exerts serious influences on the online structural temperature measurements of the spindle, which significantly affects the regression model's input. So that the estimations of the regression model can be inaccurate, and the actual thermal error will deviate from the input reference. Normally, the effect of systematic error of the feedback (model outputted thermal error) is equivalent to that of a different RITE, it usually affects the thermal error magnitude but not the STE. Few inaccurate estimations with large residuals mainly cause the thermal error to continuously deviate from the input reference, which leads to the accumulated deviations of thermal error. This is the major reason leads to occasional excessive thermal error fluctuations, even failure of the feedback control processes.

The long-term output accuracy of the thermal error model, namely the feedback accuracy, is vital for the thermal error control effect. As a matter of experimental fact, the thermal error can be stabilized for any normal speed conditions if the real-time thermal error measurement is used as feedback. However, the performance of a thermal error model cannot be ensured or reasonably estimated when facing unseen data from various work conditions, hence the thermal error stabilization level and its duration time in the feedback control processes are uncertain and instable.

We seek to address the issue of pre-estimating the reliability of feedbacks for the not-yet-in progress thermal error control process, so that we can prejudge that whether an acceptable model(regressor) can be trained with existing data and regression algorithms, or further data diversifying and cleansing, and algorithm modification are still need. A V-C (Vapnik-Chervonenkis) dimension [16] based generalization error bound [17] for the regression model is presented, by performing which the generalization error bound of feedbacks can be estimated for the not-yet-in progress thermal error control processes with high confidence.

In this study, the spindle thermal error feedback control method is first presented. Then, independence of the experimental thermal error training data is analyzed, the V-

C dimension for several thermal error models are calculated, and the generalization error bounds are estimated for the model with the confidence of 0.95. In this way the model which is most likely to give acceptable performance for unseen work conditions can be employed, the unqualified models which might output inaccurate feedbacks can be excluded, thus the risks of excessive fluctuations and failures for the thermal error feedback control processes will be largely reduced. Finally, experiments are conducted under different work conditions to verify the thermal error feedback control strategy for the mechanical spindle.

2. Thermal error feedback control based active cooling strategy for the precision spindle

2.1 The active cooling system for the spindle

The mechanical spindle of a precision boring machine is taken as the study object. The mechanical spindle isolates majority of the motor's heat generation, but the bearings still generate significant amount of heat, so that the thermal error is nonnegligible. Moreover, the mechanical spindle possesses no internal cooling channels, so an extra cooler of the mechanical spindle is needed for the experimental investigation.

2.1.1 The schematic diagram of the spindle active cooling system

The schematic diagram of the spindle active cooling system is presented in this paper is shown in Fig. 1. A Siemens S7-200 PLC is used as the controller of the system. Configuration software (Force Control) is adopted to control and monitor the cooling devices, which is run on a host computer. The coolant temperature is adjusted according to the control instruction; then, the coolant is pressurized with a recycle pump, and stabilized with a turbine flowmeter and flow control valve during the circulation. The coolant flows in the helical cooler, and finally circulates back to the coolant temperature controller.

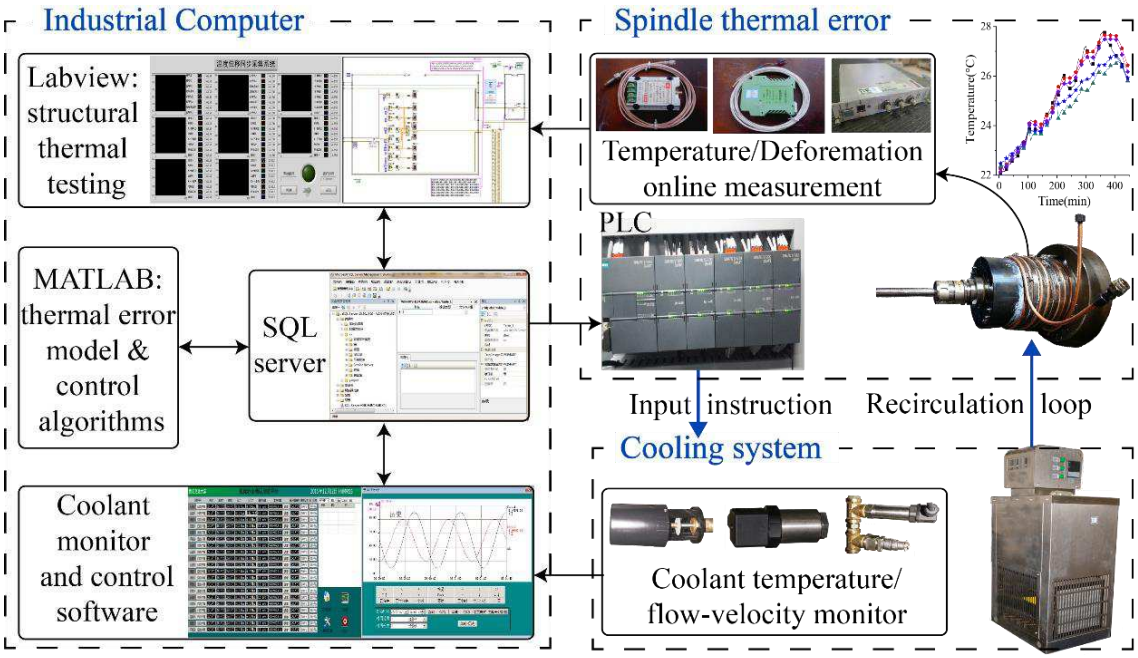

Fig. 1 Schematic diagram of the spindle active cooling system.

Temperature sensors and pressure sensors are installed in the coolant inlet and outlet of the helical cooler to monitor the coolant flow conditions, and installed on the cooling area of the spindle to measure its temperature. Data acquisition module (coolant flow velocity, pressure, temperature of the cooler inlet and outlet, structural temperature) is developed by the secondary development of Force Control configuration software, and the data exchange between the active cooling system and the host computer through the SQL Server database. Same for the data exchange between the acquisition software in host computer and the synchronous measurement system. The control module uses SQL query operation to write the latest acquired data in a table of the database and execute the feedback control algorithm. The instructions for coolant temperature (u_k) are written to another table in the database, and data in the table is then transferred to a real-time database by using ODBC router. Finally, u_k are sent to PLC of the coolant temperature controller by an I/O driver.

2.1.2 Cooler design for the mechanical spindle

Due to that the mechanical spindle of the precision boring machine possesses no inner cooling channel, an external cooling scheme is proposed. Thermal simulation for the spindle under cooling is conducted to pre-validate the external cooling scheme

before developing it. The boundary condition calculation and thermal simulation method for the spindle is referring to [12, 18]. The calculated boundary conditions and the material properties of the thermal simulation are listed in Table 1 and 2.

Table 1. Boundary conditions

	Components	Conditions	Value
Thermal contact resistance at junction	Bearing -shaft		1.603×10-4 (W/m·°C)
	Bearing-sleeve		1.778×10-4 (W/m·°C)
Thermal resistance of grease-coated joint	Cooler-housing	Chambered-flat contact	3.424×10-4 (m·°C/W)
Heating generation rate of bearings	Rear (7011C)	3000 rpm, 500N	54.54 W
	Front (7013C)	3000 rpm, 500N	86.58 W
Convective heat transfer coefficient hair	Housing -air		9.5 (W/m·°C)
Ambient temperature		Constant	16, 18 °C

Table 2. Material properties

	Specific Heat c(J/kg·°C)	Thermal conductivity k(W/m·°C)	Mass density ρ(kg/m3)	Thermal expansion $\alpha(1\times10^{-6}/°C)$
Gr15 (Bearing)	460	44	7830	12
HT250 (Housing)	510	45	7280	8.2
CuZn (Cooler)	381	401	8300	18
45Cr (Shaft)	460	44	7870	12
45# (Sleeve)	450	48	7280	11.7

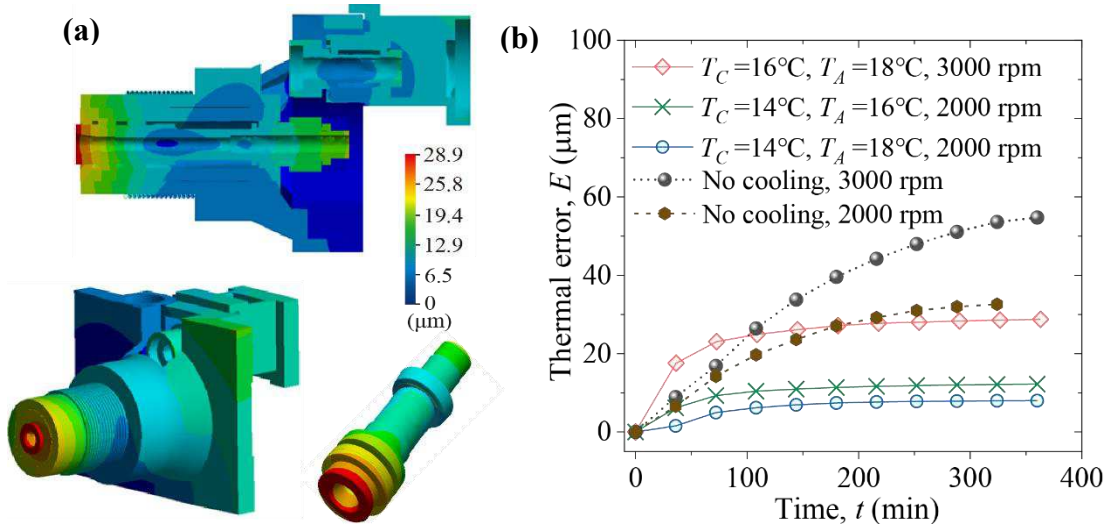

Fig. 2 Thermal deformation simulation of the spindle with helical cooler: (a). Thermal deformation field; (b) cooling effect on the spindle thermal error.

Thermal simulation results (Fig. 2) show that the external cooling largely reduces

the thermal error, the thermal error of the spindle with external cooling can easily reach stable state and has significantly superior stability than that without cooling, thus proved the effectiveness of the external cooling scheme. Then, the external helical cooler which can take effect is installed on the spindle to dissipate heat from the internal components and restrict the housing thermal deformation[11], thus suppressing the thermal error of the spindle without substantially changing the dynamic characteristics of the spindle. The helical cooler is installed and adjusted to fit the actual size and shape of the spindle, as shown in Fig. 3(a), and an insulation cover can prevent unnecessary convection heat transfer between the helical cooler and the ambient air (Fig. 3(b), (c)). Silicone-based thermal grease is fully applied on the joint surfaces to fill gaps and improve the cooling efficiency. Fig. 3(d) shows the coolant temperature controller and the recirculation loop.

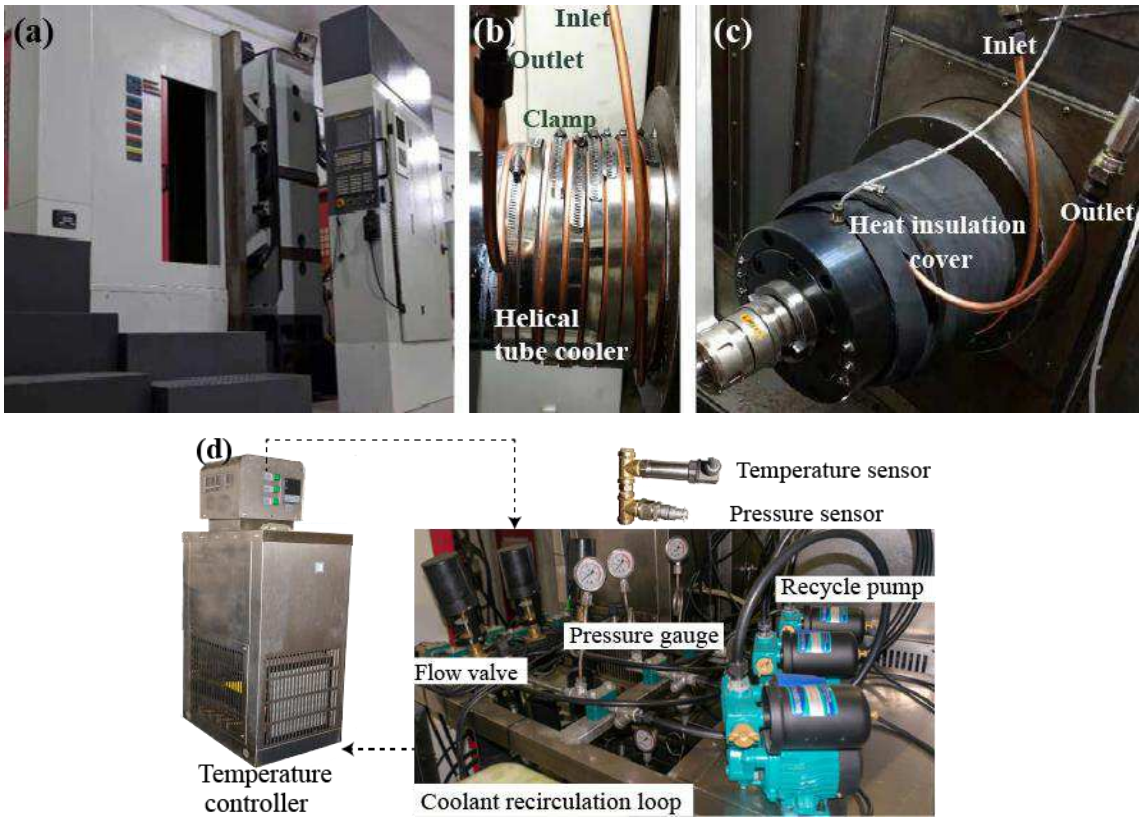

Fig. 3 The precision mechanical spindle with helical cooler: (a) machine tool; (b) installation of the helical cooler; (c) cooler with insulation; (d) the coolant temperature controller and recirculation loop.

2.2 The online synchronous thermal data testing system

The thermal behavior of the mechanical spindle can be investigated experimentally based on our previous works[19]. Synchronous temperature and displacement data are gathered by online-measurement with an acquisition card (NI SCXI-1600 series) The sampling interval in the measurement is 1 second, the precision of temperature sensor is ≤ ±0.1 °C, and the non-linearity in the displacement sensor is ≤ ±1%.

Photographs of the sensors setup and synchronous acquisition system is shown in Fig. 4. The eddy current displacement sensor directly faced the end of the spindle detection rod, so the thermal error of the spindle can be measured. Regarding the PT100 temperature sensors, T_{S1} is embedded beneath the housing and directly contacts with the spindle sleeve, T_{S2} and T_{S3} are installed on the rear of the housing. Temperature of the measuring locations which are distant from the cooler are considered as potential input feature variables for modeling, so that the influences from the temperature-varying coolant can be alleviated.

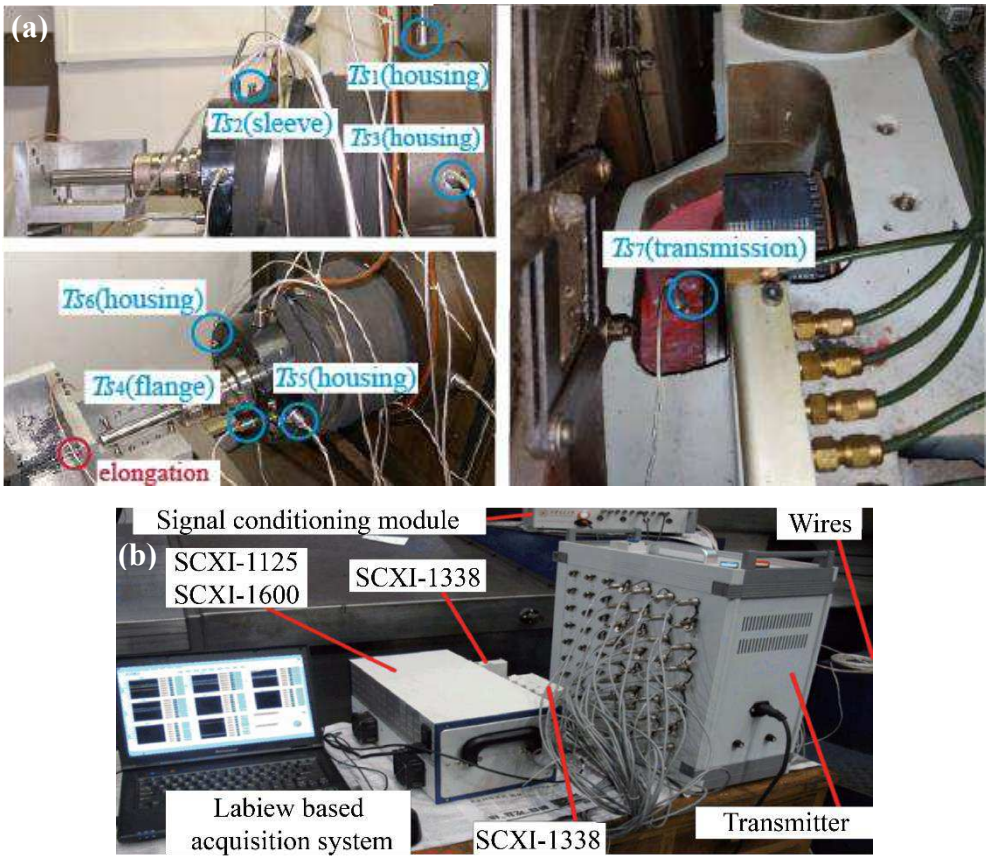

Fig. 4 Data acquisition system: (a). Sensor arrangement for the mechanical spindle; (b). Synchronous measurement system for temperature and thermal error.

The structural thermal sensitivity points for the spindle are analyzed by using Fuzzy Clustering[19], and the selected positions for temperature measuring are relatively distant from the cooler so they can be less affected. Finally, the temperature variables for thermal error modeling are optimized to be $\{T_{S1}, T_{S2}, T_{S3}, T_{S4}\}$ (Fig. 4) plus coolant temperature T_C, they are considerably strongly associated with the thermal error and relatively independent from each other. The original sampling frequency is 1Hz. In the thermal error feedback control processes, the feedback renews in every 3 minutes, and the temperature signals for every 3 minutes are processed to mean moving average for model input.

The thermal equilibrium of the spindle refers to the stable-state of its temperature field and thermal deformation field. The stability of the most concerned variable, thermal error E, can be used to determine whether the spindle is in thermal equilibrium.

2.3 Thermal error feedback control strategy

The thermal error feedback control system adopts the Proportional-Integral-Derivative (PID) algorithm. The PID-based thermal error feedback control scheme for the spindle thermal error is shown in Fig. 5.

The PID controller is given as follows,

$$u_k = u_{k0} + k_p \cdot e(t) + k_i \cdot \int_0^t e(\tau)d\tau + k_d \cdot \frac{de(t)}{dt} \tag{1}$$

where u_k is the instruction for coolant temperature (T_C is the actual value of the coolant temperature), u_{k0} is the bias and also the initial u_k value when the controlling starts, and $e_1(t)$ is the control error which equals that of RITE (Reference Input of Thermal Error) minus the estimated thermal error E. The controller parameters are the proportional gain k_p, integral gain k_i, and derivative gain k_d.

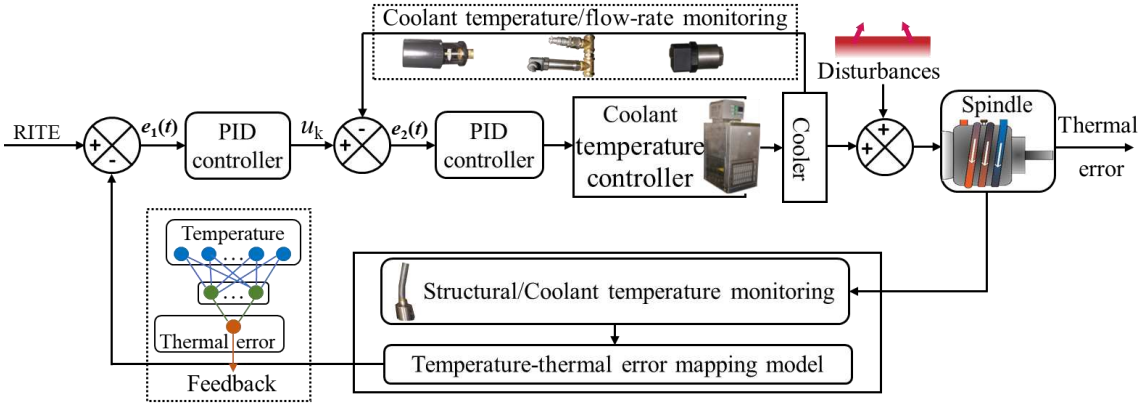

Fig. 5 Thermal error feedback control scheme

In order to tune the PID parameters, thermal error feedback control based active cooling experiments are conducted with the real-time thermal error measurements as feedbacks. Finally, the PID parameters are empirically and experimentally set to: k_p=1.5, k_i=0 and k_d=50.

3. Thermal data pre-processing and independence testing

On the basis of thermal testing experiments for the mechanical spindle, experimental thermal data including structural and coolant temperature are presented in this Section. The thermal data are cleansed by detecting and removing the outliers, and independence of the observations (data points) are tested.

3.1 Descriptive analysis of the experimental thermal data

The structural temperature $\boldsymbol{T_S}$ and coolant temperature $\boldsymbol{T_C}$ are denoted as $\boldsymbol{T_M}$=[$\boldsymbol{T_{S1}}$, $\boldsymbol{T_{S2}}$, $\boldsymbol{T_{S3}}$, $\boldsymbol{T_{S4}}$, $\boldsymbol{T_C}$], which are the explanatory variables. Thermal error $\boldsymbol{E}$ is the response variable. The active cooling experimental data for thermal error modeling includes 5 sub-datasets from different work conditions (Fig. 6). Sub-dataset 1 and 2 are obtained from the PID fine tuning experiments with real-time thermal error measuring as feedback. Sub-dataset 3, 4 and 5 are measured in early experimental attempts of thermal error feedback controlling, in which the thermal error model (for outputting feedback) is trained with insufficient and limited data. The experimental data of sub-dataset 1~5 can well reflect the effect that the coolant of rapidly-varying temperature act on the structural temperature and thermal error of the spindle. Above experiments are all

conducted in constant-temperature environment and with similar cool-down time, so the influences from the ambient temperature and initial structural temperature/deformation field is trivial.

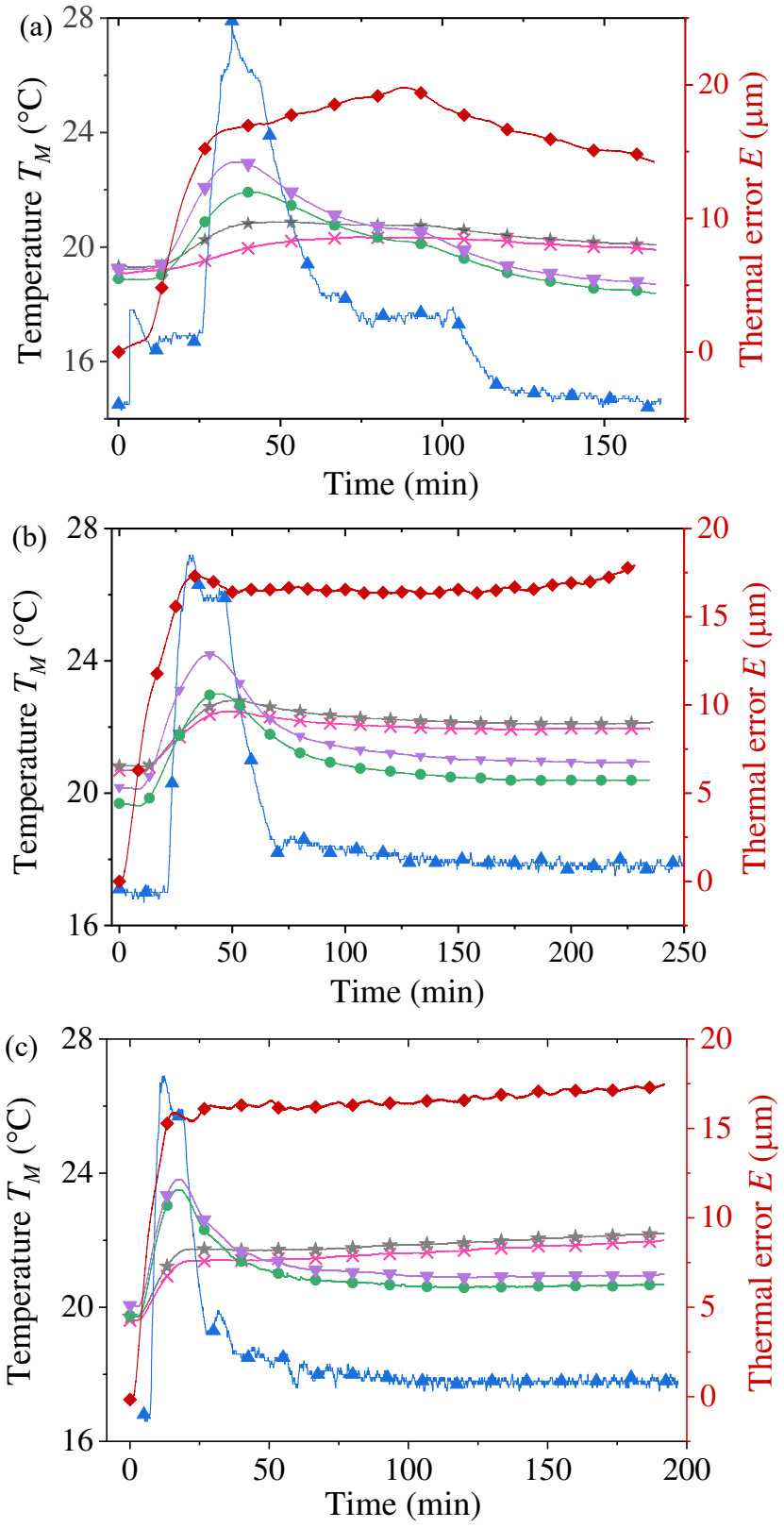

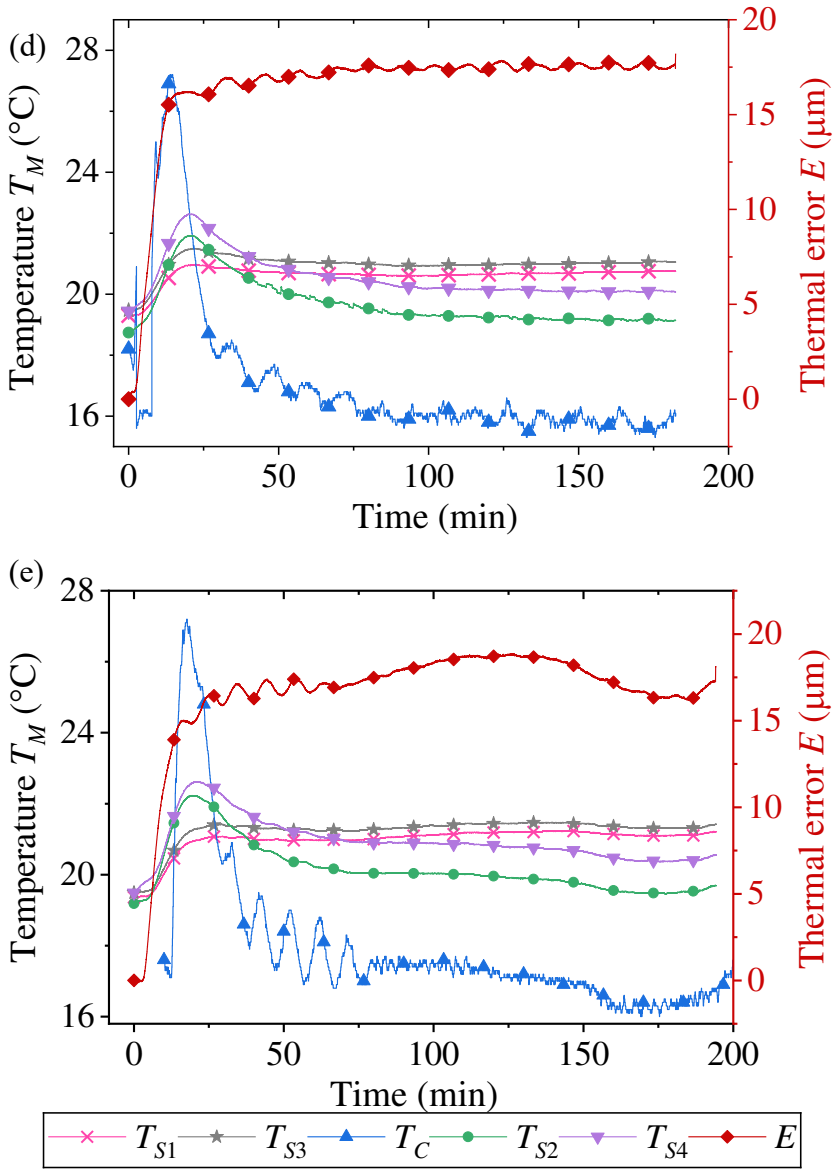

Fig. 6 Experimental data (3000 rpm, initial T_C=16°C) for training the thermal error model: (a) Sub-dataset 1; (b) Sub-dataset 2; (c) Sub-dataset 3; (d) Sub-dataset 4; (e) Sub-dataset 5.

The spindle structural temperature and deformation field (thermal state), relates strongly to the previous thermal state, the observations in Fig. 5 are obviously dependent and associated. But it is unclear whether the data of the thermal state variations are independent. For all above thermal data, we denote each of their variation datapoints(observations) at time t as: $\boldsymbol{D}_t$=[$\boldsymbol{T_M}$, $\boldsymbol{E}$]$_t$-[$\boldsymbol{T_M}$, $\boldsymbol{E}$]$_{t-1}$, t=2,3,…, T. The thermal variation data are denoted as $\boldsymbol{D}$. The mean and variance of each variable vector ($\Delta\boldsymbol{T_{S1}}$, $\Delta\boldsymbol{T_{S2}}$, $\Delta\boldsymbol{T_{S3}}$, $\Delta\boldsymbol{T_{S4}}$, $\Delta\boldsymbol{T}$C, $\Delta\boldsymbol{E}$) is calculated and compared among time-periods and sub-datasets, and they are found to be close in value, so each column of $\boldsymbol{D}$ can be regarded as stationary data. Finally, the thermal error E_t at any timepoint t can be estimated by

summing $\Delta \boldsymbol{E}$:

$$E_t = \sum_{i=1}^{t} \Delta E_i \tag{2}$$

3.2 Boosting based outliers detection for the thermal data

The Boosting based Outliers Detection approach is employed for cleansing the outliers for dataset $\boldsymbol{D}$ [19]. The training dataset $\boldsymbol{D}$ and a robust SVR weak learner are given first, and the algorithm requires a maximum number of iterations M to be chosen a prior. In each iteration step $I \in \{1,\ldots, M\}$, training sample at this iteration is randomly drawn from $p^I=\{p_1^I, p_2^I, \ldots, p_n^I\}$, with replacement according to the normalized probability weights distribution $\boldsymbol{D}$, which is a sample $\boldsymbol{D}^I$ of size n. And the SVR regression function f^I is established with the sample $\boldsymbol{D}^I$. The initial iteration step I is set to one and the initial probability weights And the SVR regression function f^I is established with the sample $\boldsymbol{D}^I$. The initial iteration step I is set to one and the initial probability weights p^I are $\{\frac{1}{n},\ldots,\frac{1}{n}\}$. initial f^I is estimated using the initial probability weights p^1. Then, at every iteration I, $I>1$, the updated p^I would be normalized, and the regression model f^I is established according to the normalized p^I. The model f^I would be evaluated by using an overall error measure, which is calculated on the basis of regression error rates $e_1^I, e_2^I,\ldots, e_n^I$ at each iteration I. Error rate $e_i^I, i \in \{1, 2 ,\ldots, n\}, I \in \{1,2,\ldots,M\}$ is defined as：$\frac{y_i - f^I(x_i)}{y_i}$.

The regression error rates are given by dividing the absolute residuals by the data point value, such that the error rate e_i^I of every data point is obtained and lies in the interval [0,1]. Then the error rate of every data point is compared with the preset error rate threshold τ, and the data points whose error rates exceed the threshold τ are considered as the poorly estimated. Finally, the overall error measure ε^I at iteration I is calculated as:

$$\varepsilon^I = \sum_{\{i:e_i^I > \tau\}} p^I \tag{3}$$

where $i \in \{1,2,\ldots,n\}$, and e_i^I is the absolute residual of the ith data point. The

calculated overall error ε^I is the weighted sum of the normalized error rate which also lies in the interval [0,1]. The probability weights are updated according to a rule depending on threshold τ. The weights associated with data points with residuals smaller than are decreased, while the weights of poorly estimated data points with residuals larger than would remain constant. The weights of well estimated data points are decreased as $\beta^I \leftarrow (\varepsilon^I)^r$, and $p_i^I \leftarrow p_i^I \cdot \beta^I$, where r is the power coefficient which controls the decreasing rate of the weights for well estimated data points.

After the probability weights of data points for iteration I+1 are updated, the updated probability weight distribution of iteration I+1 would be normalize so the sum is 1, and the probability weights of the poorly data points would be in fact increased. Iterations would stop when overall error rate ε^I is low enough, or after the algorithm has iterated M times.

Finally, three data points are suspected as outliers because they are associated with prominent large normalized probability weights: 0.1722, 0.1638 and 0.2414, while the largest normalized weight for the other training data points is 0.0511. The dataset $\boldsymbol{D}$ is cleansed by removing these data points of suspected outliers.

3.3 Independence testing for the spindle thermal data

The lagged autocorrelation and portmanteau statistic are adopted to characterize the independence of the multidimensional spindle thermal dataset, in order to determine whether the independence hypothesis based algorithms are appropriate to be applied.

3.3.1 The multivariate portmanteau statistic

The measured and preprocessed spindle thermal data matrix $\boldsymbol{D}$ can be denoted as a multivariate vector($T \times S$):

$$\boldsymbol{D} = \begin{bmatrix} x_{11} & x_{12} & \cdots & x_{1S} \\ x_{21} & x_{22} & \cdots & x_{2S} \\ \cdots & \cdots & & \cdots \\ x_{T1} & x_{T2} & \cdots & x_{TS} \end{bmatrix} \tag{4}$$

where S is the total number of variates, T is the total number of total observations, s and

t are respectively the coordination for variate and observation (x_{ts}). $\boldsymbol{D_{t:T-l}}$ denotes the *t*th to (*T*-*l*)th observations, $\boldsymbol{D_{t+l:T}}$ contains the (*t*+*l*)th to *T*th observations.

Denoting the diagonal matrix of standard deviations by $\boldsymbol{S_\sigma}$=Diag(σ_1, σ_2, σ_S), where σ_s is the standard deviation of the *s*th variate x_s, $\sigma_s=\sqrt{T^{-1}\sum_{t=1}^{T}x_{ts}}$. $\boldsymbol{R_l}$ is the cross-correlation for $\boldsymbol{D_{t:T-l}}$ and $\boldsymbol{D_{t+l:T}}$, $\boldsymbol{C_l}$ is the autocovariance matrix at lag *l*:

$$\boldsymbol{C_l} = \boldsymbol{S_\sigma R_l S_\sigma} = \begin{bmatrix} \sigma_1 & 0 & \dots & 0 \\ 0 & \sigma_2 & \dots & 0 \\ \dots & \dots & \dots & \dots \\ 0 & 0 & \dots & \sigma_d \end{bmatrix} \begin{bmatrix} Ex_1x_1 & Ex_2x_1 & \dots & Ex_Sx_1 \\ Ex_1x_2 & Ex_2x_2 & \dots & Ex_Sx_2 \\ \dots & \dots & \dots & \dots \\ Ex_1x_S & Ex_2x_S & \dots & Ex_Sx_S \end{bmatrix} \begin{bmatrix} \sigma_1 & 0 & \dots & 0 \\ 0 & \sigma_2 & \dots & 0 \\ \dots & \dots & \dots & \dots \\ 0 & 0 & \dots & \sigma_S \end{bmatrix} \tag{5}$$

Then, the portmanteau statistic *Q* is defined[20, 21]:

$$Q = T^2 \sum_{l=1}^{L} (T-l)^{-1} \left(\boldsymbol{C}_l^{\,T} \boldsymbol{C}_0^{\,-1} \boldsymbol{C}_l \boldsymbol{C}_0^{\,-1} \right)^T \tag{6}$$

3.3.2 Independence testing for the spindle thermal data

The *S* variates of $\boldsymbol{D}$ are the variations of structural temperature ΔT_S and coolant temperature ΔT_C, and the thermal error ΔE. The independence testing is repeated with *l*=1: 150. In each test, $\boldsymbol{D_{t:T-l}}$ and $\boldsymbol{D_{t+l:T}}$ are normalized to a (0, σ^2) distribution.

The null distribution (independent) is approximated using the inversed cumulative distribution function of standard γ distribution:

$$g(l) = \left(\frac{\int_0^l t^{\gamma-1} e^{-t} dt}{\int_0^\infty t^{\gamma-1} e^{-t} d} \right)^{-1}, l \geq 0, \gamma > 0 \tag{7}$$

For each lag *l*, the null hypothesis of independence is supported if $Q<g(l)$. $Q>g(l)$ means that the null hypothesis is rejected, the larger *Q* means the stronger violation for the independence hypothesis of the tested data. *Q* against different lag *l* (*l*=1:150) is calculated for the thermal data of the spindle under active cooling (Dataset I). Thermal data of the precision spindle without cooling (Dataset II), which is repeatedly adopted in thermal error modeling and proved high-quality [13, 22, 23], their *Q* against same lags (*l*=1:150) are also calculated for comparison. Finally, in order to test the data independence, *Q* of the above datasets are compared with that of the inversed

cumulative distribution function which is standard γ distribution (Fig. 7).

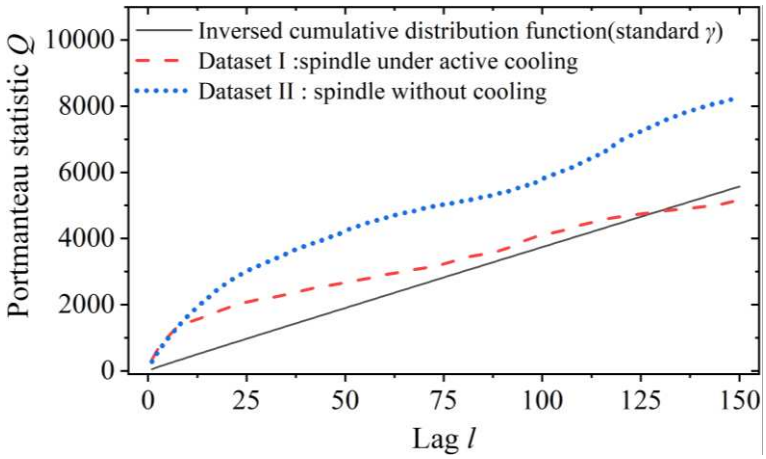

Fig. 7 Experimental data for training the thermal error model

For the thermal Dataset I (spindle under active cooling), the IID hypothesis is supported in 18 of 150 values, and the Q curve is close to that of the inversed cumulative distribution function (standard γ distribution), so there is only slight violation to the null hypothesis (Fig. 7). The violation for independence assumption of the Dataset I is much weaker than that of the Dataset II (spindle without cooling). In view of the fine modeling effect with Dataset II using independence-based algorithms, we conclude that the independent violation is weak enough to be ignored for Dataset I.

4. Thermal error modeling and reliability pre-estimation of the feedback

As is analyzed in Section 3.3, the independence assumption based algorithms are appropriate to be applied on the dataset $\boldsymbol{D}$ (Dataset I). The regression modeling algorithms are performed to established thermal error models, then the generalization bounds of the models are estimated. Finally, the model which is most likely to give acceptable performance for unseen work conditions is employed, and the maximum T_C deviation (from the ideal T_C) for the upcoming thermal error feedback control processes is pre-estimated.

4.1 Regression modeling algorithms for the thermal error modeling

4.1.1 Support vector machine for regression theorem

In the regression context of SVM, the training dataset is ($\boldsymbol{X}_i$, Y_i), i=1,2,…,n, where $\boldsymbol{X}$ is a S-dimensional input, and $\boldsymbol{X}\in\boldsymbol{R}^{\boldsymbol{S}}$. The Y is a one-dimensional output and $Y\in R$. In SVR, the input $\boldsymbol{X}$ is mapped onto a high dimension feature space using a kernel function at first, then a model is established in this high dimension feature space[24-26]. The multi-variates linear model $f(\boldsymbol{X_i},\Omega)$ is given by:

$$f(\boldsymbol{X}_i,\Omega)=\sum_{k=1}^{m}\omega_k g_k(\boldsymbol{X}) \tag{8}$$

where $g_k(\boldsymbol{X})$ denotes a set of nonlinear transformations, ω is the set of variable coefficients in the multi-linear model, and $\Omega=\{\omega_1, \omega_2, ..., \omega_n\}$. The quality of estimation of the established model is measured by the loss function $L(Y, f(\boldsymbol{X}_i, \Omega))$. SVR uses the ε-insensitive loss function:

$$L(Y,f(\boldsymbol{X}_i,\Omega))=\begin{cases}0 & \text{if } |Y-f(\boldsymbol{X},\Omega)|\le\varepsilon\\ |Y-f(\boldsymbol{X},\Omega)|-\varepsilon & \text{otherwise}\end{cases} \tag{9}$$

where the parameter ε defines the width of insensitive margin. The empirical risk is:

$$R_{emp}=\frac{1}{n}\sum_{i=1}^{n}L(Y_i,f(\boldsymbol{X}_i,\Omega)) \tag{10}$$

SVR model is established by minimizing:

$$\begin{aligned}&\min\frac{1}{2}\|\Omega\|^2+C\sum_{i=1}^{n}(\xi_i+\xi_i^*)\\ &s.t.\begin{cases}y_i-f(\boldsymbol{X}_i,\Omega)\le\varepsilon+\xi_i\\ f(\boldsymbol{X}_i,\Omega)-y_i<\varepsilon+\xi_i^*\\ \xi_i,\xi_i^*\ge 0, i=1,...,n\end{cases}\end{aligned} \tag{11}$$

In the minimization problem (1), ε defines the width of the insensitive margin (tolerance margin), and ξ is called “slack variable” which determines the deviation distances from the insensitive margin. C is the penalty that characterizes the amount of tolerance for the data points lying outside the insensitive margin[27]. The function f is as follows,

$$f = \sum_{i=1}^{l} \alpha_i K(\boldsymbol{X}_i, \boldsymbol{X}_j) + b \tag{12}$$

where $K(\boldsymbol{X}_i, \boldsymbol{X}_j)$ is the kernel function which is the inner product of the high-dimensionally mapped input feature vectors, $K(\boldsymbol{X}_i, \boldsymbol{X}_j)=\Phi(\boldsymbol{X}_i)^{\mathrm{T}}\Phi(\boldsymbol{X}_j)$. Kernel function makes the dot product calculation practical, and it can be considered as a measure of similarity among the training data. Many kernel forms are commonly used in SVR, and the radial basis function (RBF) kernel function is adopted for SVR:

$$K(\boldsymbol{X}_i, \boldsymbol{X}_j) = \exp(-\frac{\| \boldsymbol{X}_i - \boldsymbol{X}_j \|}{2\gamma^2}), \text{if } \ i \neq j \tag{13}$$

where γ is the (Gaussian) kernel width parameter.

Moreover, the ε-insensitive zone width parameter ε is already empirically set to 0.01, and the SVR model is established with two parameters, the penalty parameter C and the RBF kernel width parameter γ. The GA method is adopted to optimize the parameters of penalty parameter C and RBF kernel width parameter γ[19]. The GA is based on the mechanics of natural selection and genetics. Procedures of GA in this paper are carried out using references[28], which involves three stages, (1) population initialization, (2) operators and (3) chromosome evaluation.

4.1.2 Random Forrest Regression Theorem

A random forest regression (RFR) model[29, 30] consists a collection of classification and regression trees (CART)[31]. Two random sampling procedures are adopted in RFR to alleviate over-fitting:

1. Bootstrap aggregating. For each CART a different sub-dataset is used for training and one-third of the training data (out-of-bag data, OOB) are used for estimating the general error. By sampling with replacement, some observations may be repeated in each subset. Finally, the CARTs are ensembled by averaging the output.

2. Feature projection. At first, certain number of input variables are randomly selected for the tree training process, and the data subset of the randomly selected input variables are then used to split each node, which results in less correlation among trees and a lower error rate.

Above procedures can largely reduce the variance error of RFR, but the bias can

still be significant. Application of the bias-correction procedure can alleviate this problem[30, 32] by estimating the systematic residuals and subtract them from the estimation:

1. Fit the training dataset using RFR. Compute the estimated values and residuals $r=y-y^*$, where r is the residual, y is the test value and y^* is the RFR models' estimation with input $\boldsymbol{X}$.

2. Fit a RFR model regarding r as the response variable (explanatory variables are also $\boldsymbol{X}$), output of the model is r^*, and the final estimation output y_o is:

$$y_o = y^* + r^* \tag{14}$$

4.2 Generalization bounds estimation via V-C dimension

4.2.1 Estimating the V-C dimension

Let X be the explanatory variable leading to the response variable Y, and the assuming (X, Y) values are on the $\chi \times Y$. $\alpha_k \in \Lambda$, $k=1, \ldots, K$, Λ is an index set for the regression functions, and the hypothesis space is finite, so the regression function is denoted as $Y=f(X, \alpha_k)$. Let $\boldsymbol{D}$ be the randomly sampled dataset with the length of $2n_l$, ($Z_1=(X_1, Y_1)$, $Z_2=(X_2, Y_2)$, …, $Z_{2nl}=(X_{2n_l}, Y_{2n_l})$) be a data set of size $2n_l$ of independent and identically distributed copies of (X, Y). Write $\boldsymbol{D_1}=((X_1, Y_1), (X_2, Y_2), \ldots, (X_{n_l}, Y_{n_l}))$ for the first half and $\boldsymbol{D_2}=(Z_{nl+1}=(X_{n_l+1}, Y_{n_l+1}), Z_{nl+2}=(X_{n_l+2}, Y_{n_l+2}), \ldots, Z_{2nl}=(X_{2n_l}, Y_{2n_l}))$ for the second half of $\boldsymbol{D}$. Data length of $\boldsymbol{D_1}$ and $\boldsymbol{D_2}$ are all n_l.

Let $L(\alpha_k)$ be the unknown true loss of the function f at α_k, $Q((X_i, Y_i), \alpha)=(Y_i-f(X_i, \alpha))^2$ be the bounded real-value loss function. For a fixed α, the value of $Q((X_i, Y_i), \alpha)$ is within $[0, B)$, where B is the upper bound of the losses. Discretize $Q((X_i, Y_i), \alpha)$ using m disjoint intervals:

$$Q^m((X,Y),\alpha) = \sum_{j=0}^{m-1} \frac{(2j+1)B}{2m} I(Q((X,Y),\alpha)) \tag{15}$$

$$I(Q((X,Y),\alpha)) = \begin{cases} 1, & \text{if } Q((X,Y),\alpha) \in [\frac{jB}{m}, \frac{(j+1)B}{m}) \\ 0, & \text{otherwise} \end{cases} \tag{16}$$

where I is an indicator function taking value 1 when its argument is true and value 0 when it is false; the discretization is based on the uniform left-closed, right-open partition of [0, B) into m subintervals, here denoted $[\frac{jB}{m}, \frac{(j+1)B}{m})$, which are the midpoints.

Let α_1, $\alpha_2 \in \Lambda$, and v be the empirical loss function, so the empirical functions on the first and the second half of the training data ($\boldsymbol{D}_1$ and $\boldsymbol{D}_2$) are:

$$v(\boldsymbol{D}_1, \alpha_2) = \frac{1}{n}\sum_{i=1}^{n} Q((X_{n+1}, Y_{n+1}), \alpha_2) \tag{17}$$

$$v(\boldsymbol{D}_2, \alpha_1) = \frac{1}{n}\sum_{i=1}^{n} Q((X_{n+1}, Y_{n+1}), \alpha_1) \tag{18}$$

Based on formula (15), we introduce the empirical counts of the data points whose losses belongs to $[\frac{jB}{m}, \frac{(j+1)B}{m})$, which can be written as:

$$C_j^m(\boldsymbol{D}_1, \alpha_2) = \sum_{i=1}^{n} I(Q((X_{n+1}, Y_{n+1}), \alpha_2)) \tag{19}$$

$$C_j^m(\boldsymbol{D}_2, \alpha_1) = \sum_{i=1}^{n} I(Q((X_{n+1}, Y_{n+1}), \alpha_1)) \tag{20}$$

This means we are counting the errors of the α_1 model on the second half of the data($\boldsymbol{D}_2$) and the errors of the α_2 model on the first half of the data($\boldsymbol{D}_1$). This begins the set up of the cross-validation form of the error that we use and leads to the following expressions for the empirical losses of the discretized loss functions:

$$v^m(\boldsymbol{D}_2, \alpha_1) = \frac{1}{n}\sum_{i=1}^{m-1} C_j^m(\boldsymbol{D}_2, \alpha_1)\frac{(2j+1)B}{2m} \tag{21}$$

$$v^m(\boldsymbol{D}_1, \alpha_2) = \frac{1}{n}\sum_{i=1}^{m-1} C_j^m(\boldsymbol{D}_1, \alpha_2)\frac{(2j+1)B}{2m} \tag{22}$$

and the empirical loss in the jth discretized subinterval is:

$$v_j^m(\boldsymbol{D}_2, \alpha_1) = \frac{1}{n} C_j^m(\boldsymbol{D}_2, \alpha_1)\frac{(2j+1)B}{2m} \tag{23}$$

$$v_j^m(\boldsymbol{D}_1, \alpha_2) = \frac{1}{n} C_j^m(\boldsymbol{D}_1, \alpha_2)\frac{(2j+1)B}{2m} \tag{24}$$

Referring to, with the $\varepsilon \geq 0$, $m \in ¥$ and j=0,1, …, m-1 and the V-C dimension

$d_{VC}\{L(\cdot, \alpha): \alpha \in \Lambda\}$ is finite, the expected maximum difference between the empirical losses Δ is:

$$\Delta = E(\sup_{\alpha_1,\alpha_2 \in \Lambda} |v_j^m((X_{n+1:2n}, Y_{n+1:2n}), \alpha_1) - v_j^m((X_{1:n}, Y_{1:n}), \alpha_2)|) \quad (25)$$

where sup() means the support functions of v_j^m.

$\delta_{d_{VC}}(n_l)$ is the upper bound for Δ of each sub-dataset ($\boldsymbol{D_1}$ and $\boldsymbol{D_2}$ for each n_l):

$$\delta_{d_{VC}}(n_l) = c\sqrt{\frac{d_{VC}}{n_l}\log(\frac{2n_l e}{d_{VC}})} \quad (26)$$

where c is a constant empirically chosen to 8.

We design a series of data length n_t (t=1, 2, …, T) for randomly sampling sub-datasets. For each t=1, 2, …, T, a bootstrap sample $\boldsymbol{D}$ of size $2 \cdot n_t$ is picked, and is randomly divided into 2 sub-datasets $\boldsymbol{D_1}$ and $\boldsymbol{D_2}$. Two regression functions are respectively trained on $\boldsymbol{D_1}$ and $\boldsymbol{D_2}$, which are denoted as $f(\alpha_1)$ and $f(\alpha_2)$. The loss function is estimated by computing the squared error $SE_1=(f(x_1, \alpha_2)-y_1)^2$, $SE_2=(f(x_2, \alpha_1)-y_2)^2$. For the m discretized subintervals, empirical counting $C_j^m(\boldsymbol{D_2},\alpha_1)$ and $C_j^m(\boldsymbol{D_1},\alpha_2)$ for each subinterval are obtained using the squared error SE_1 and SE_2 (eqs. (19)~(20)), and $v_j^m(\boldsymbol{D_2},\alpha_1)$ and $v_j^m(\boldsymbol{D_1},\alpha_2)$ can be estimated.

The bootstrapping method is used to iteratively resample a dataset with replacement, and estimate the statistics. In the bootstrapping, an observation for $\delta_{d_{VC}}$ is introduced, which is denoted as $\delta^*_{d_{VC}}$. The $\delta^*_{d_{VC}}$ for each bootstrap sample $\boldsymbol{D}$ can be obtained by taking the mean and sum across all subintervals.

$$\delta^*_{d_{VC}}(n_l) = \sum_{j=1}^{m-1} \text{mean}|v_j^m(\boldsymbol{D}_1, \alpha_2) - v_j^m(\boldsymbol{D_2}, \alpha_1)| \quad (27)$$

Finally, the V-C dimension d_{VC} can be obtained by minimizing the squared distance (f_{n_t}) between the observation $\delta^*_{d_{VC}}(n_t)$ and the true upper bound $\delta_{d_{VC}}(n_t)$,

$$f_{n_t}(d_{VC}) = \sum_{t=1}^{T}\left(\delta^*_{d_{VC}}(n_t) - \delta_{d_{VC}}(n_t)\right)^2 = \sum_{l=1}^{L}\left(\delta^*_{d_{VC}}(n_t) - c\sqrt{\frac{d_{VC}}{n_t}\log(\frac{2n_t e}{d_{VC}})}\right)^2 \quad (28)$$

4.2.2 Loss estimation for the regression function

Let $Q_{emp}(\alpha_k)$ be the empirical risk at α_k. For any $p \in (0, 1)$, with probability at least 1-p the inequality[17, 33] is:

$$Q(\alpha_k) \le Q_{emp}(\alpha_k) + m\sqrt{\frac{1}{n}\log((\frac{2m}{p})(\frac{2ne}{d_{VC}})^{d_{VC}})} \quad (29)$$

where the empirical risk $Q_{emp}(\alpha_k)$ is defined as the sum squared error of the fitting *MSE* of the function $f(\alpha_k)$ on the training dataset:

$$Q_{emp}(\alpha_k) = \sqrt{\frac{1}{n}\sum_{i=1}^{n}(y_i^* - y_i)^2} \quad (30)$$

where y^* is the prediction, and y is the measured data for the response variable Y. Besides, the Vapnik–Chervonenkis (V-C) dimension d_{VC} needs to be calculated for estimating the upper bound of $Q(\alpha_k)$. The best model is the one which minimizes $Q(\alpha_k)$.

The GA-SVR and RFR regression algorithms are employed to establish the thermal error models with the experimental data presented in Section 3.1. Then the generalization error bound estimating approach is applied on the established models. With p=0.05 (probability 1-p equals 0.95), the bounded loss function is discretized into 10 disjoint intervals, and the d_{VC}, Q_{emp} and Q are calculated and listed in Table 3.

Table 3. Models evaluation results

	m	d_{VC}	Q_{emp}	Q
MLR	10	6	0.2379	0.7342
GA-SVR	10	5	0.1402	0.6882
RFR	10	5	0.1270	0.6211

With the probability of 0.95, the upper bounds (absolute value) of generalization error for the MLR, GA-SVR and RFR models are respectively 0.7342μm, 0.6882μm and 0.6211μm (Table1).

4.2.3 Reliability pre-estimation for the thermal error feedback control

Generalization error bound of the RFR model is the smallest among the three models, thus the feedback accuracy with the RFR model is expected to be the highest for unseen conditions.

Normal systematic residual of the feedback (E) is equivalent to a different RITE, so it usually affects the thermal error magnitude but not the STE. Few inaccurate variations (ΔE) estimations with large residuals at certain time-points are the major cause for the T_C deviations (from the ideal T_C) and excessive thermal error fluctuations. But, if the estimation residual of ΔE is bounded to a small range, only small fluctuations and slight sustained increment/decrement tendencies will occur, even if the estimation residual accumulates for a period. The experimentally tuned proportional gain k_p is 1.5, so the maximum T_C deviation is expected to be 0.93℃ with the RFR model. We can assume that the thermal error will be stabilized to be within an acceptable range in the thermal error feedback control processes.

5. Experiments of the thermal error feedback control based spindle active cooling

5.1 Pre-determination of RITE

Adjusting and maintaining coolant temperature consumes major energy in the active cooling for spindle. The magnitude of RITE mainly affects the total energy consumption of the thermal error controlling process and will slightly affect STE. Maintaining STE at a relatively high thermal error value can reduce the amount of heat that needs to be dissipated by coolant circulations, thus decreasing the energy consumption of adjusting T_C in the coolant temperature controller.

In the constant temperature cooling, the ambient temperature and the initial temperature of the spindle structure are 18℃. Minimum energy would be consumed in heat convection with ambient air if T_C keeps close to 18℃, and an instruction(u_k) for coolant temperature (T_C) that is distant from 18℃ leads to energy consumption in the coolant temperature controller. Thus, coolant temperature should be close to 18℃ in the control process so the energy consumption is low. Regarding the cooling with constant 16℃, the pre-heating time is about 120 min until thermal error tends to stabilize. Then, for the thermal error feedback controlling with rotation speed of 3000 pm, RITE is empirically determined to be 17μm where the coolant temperature changes

around 16℃. As for the thermal error feedback controlling with rotation speed of 2000 rpm, RITE is set to 12μm where the coolant temperature also varies around 16℃.

5.2 Evaluation method of STE

In order to quantitatively evaluate the STE using discrete derivative, the fluctuation in the measured thermal error curves should be avoided such that only the major variation trend of the thermal error will be reflected[12]. The spindle thermal error which varies non-linearly with time is fitted to a smooth curve:

$$f(t) = p_5 \cdot t^4 + p_4 \cdot t^3 + p_3 \cdot t^2 + p_2 \cdot t + p_1 \tag{31}$$

The least square method is used to fit the 4-order polynomial regression model. STE is the discrete derivative of fitted thermal error $f(t)$ to time t:

$$\mathrm{STE} = df(t) / dt \tag{32}$$

In practical applications, a precision machine tool is normally pre-heated before machining. The spindle thermal deformation induced error in machining is ignorable when the thermal error is stable, because most of the spindle thermal error will be compensated by tool-setting. The thermal error can be regarded as stable when STE becomes less than a threshold value.

5.3 Experimental results of the thermal error feedback control

In the active cooling experiments, the thermal error feedback control strategy is performed on the mechanical spindle under rotation speed conditions which are similar with that in common boring machining. Each experiment is conducted after the spindle is cooled down in natural environment (uncontrolled environmental temperature), so the season and weather would affect the initial temperature/thermal deformation distribution of the spindle structure, hence the different spindle thermal behavior in the experiments under same work condition. Five experiments are conducted in continuous days of winter, and the ambient temperature is within 18 ± 1℃ for all the experiments. In the active cooling experiments, the initial temperature (T_{S0}) distribution of the spindle structure is assumed to be uniform, but T_{S0} varies in different experiments due to

different weather, season and cool-down time. As a result, the thermal experiment results of the spindle might be different due to different T_{S0} under same work condition.

Case 1 and 2 is conducted under work condition #1 of constant rotation speed of 3000rpm. Case 3 and 4 are conducted under work condition #2: the mechanical spindle operates at 3000rpm before 80min, at 2000rpm before 140min, and at 4000rpm until the end. Case 5 is conducted under work condition under work condition #3: the mechanical spindle operates at 3000rpm before 80min, at 4000rpm before 140min, and at 2000rpm until the end. The experimental results of the thermal error feedback control based active cooling are presented in Fig. 8, they are compared with the experimental results of cooling with constant 16℃. In this way, the robustness of the thermal error feedback control strategy can be tested.

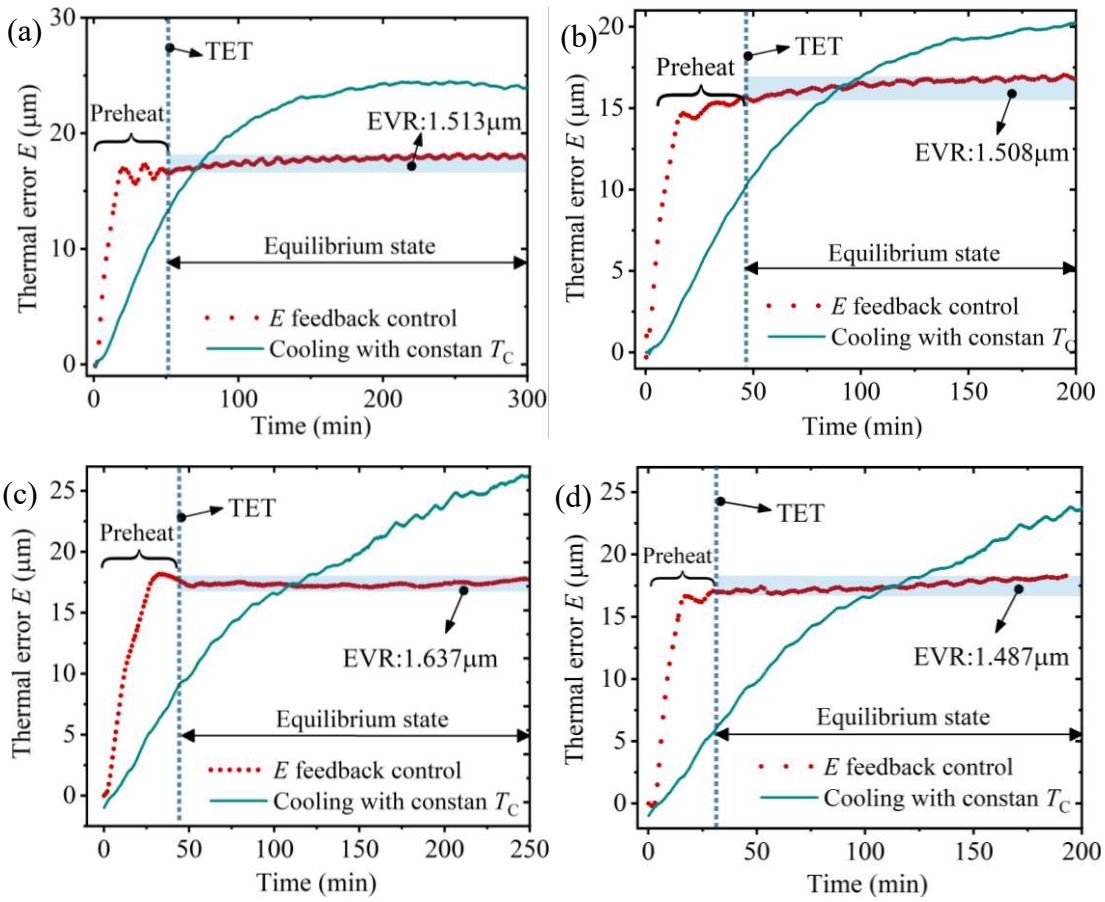

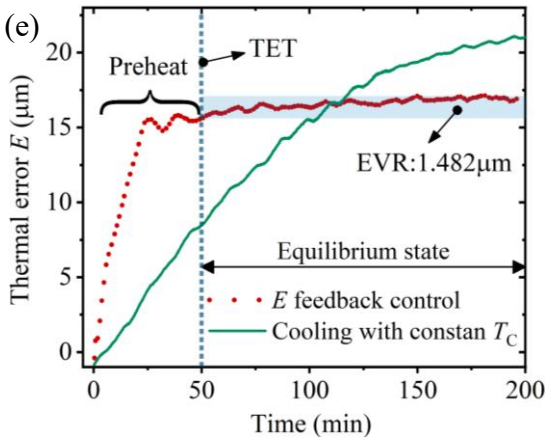

Fig. 8 Experimental results of the thermal error feedback control: (a) Case1(Work condition #1, T_{S0}=18.3℃); (b) Case2(Work condition #1, T_{S0}=17.7℃); (c) Case3(Work condition #2, T_{S0}=18.1℃); (d) Case4(Work condition #2, T_{S0}=18.6℃); (e) Case5(Work condition #3, T_{S0}=18.5℃).

The E curves with constant temperature cooling (T_C=16 ℃) rose steadily in the entire experiment process (Fig. 8), while the E curve with thermal error feedback control stabilized around the pre-set RITE (17μm) after preheating of 30~50 minutes. For the experiments in Fig. 12, the temperature data (sampling frequency is 1Hz) of every 3 minutes are characterized to a single mean moving average value, so the model outputted feedback value renews in every 3 minutes. The thermal errors measurements are fitted to smooth curves using five-order polynomial regression method, so the STE which reflect the major variation trend can be obtained (Fig. 9). The fitted E polynomials are presented in Table 4.

Table 4. Coefficients of the fitted polynomials

	Case 1	Case 2	Case 3	Case 4	Case 5	T_C=16℃
p_1	7.331×10^{-21}	1.034×10^{-19}	1.387×10^{-17}	2.231×10^{-19}	1.154×10^{-18}	-4.305×10^{-21}
p_2	-4.724×10^{-16}	-2.78×10^{-14}	2.881×10^{-13}	-8.01×10^{-15}	4.234×10^{-14}	-3.937×10^{-17}
p_3	1.193×10^{-16}	2.821×10^{-10}	2.335×10^{-9}	1.074×10^{-10}	5.927×10^{-10}	1.322×10^{-11}
p_4	-1.516×10^{-7}	-1.378×10^{-6}	9.051×10^{-6}	6.426×10^{-7}	3.917×10^{-6}	-3.951×10^{-7}
p_5	0.001039	0.003657	0.01651	0.001775	0.01234	0.005098
p_6	14.59	13.84	6.115	15.24	2.22	-2.134

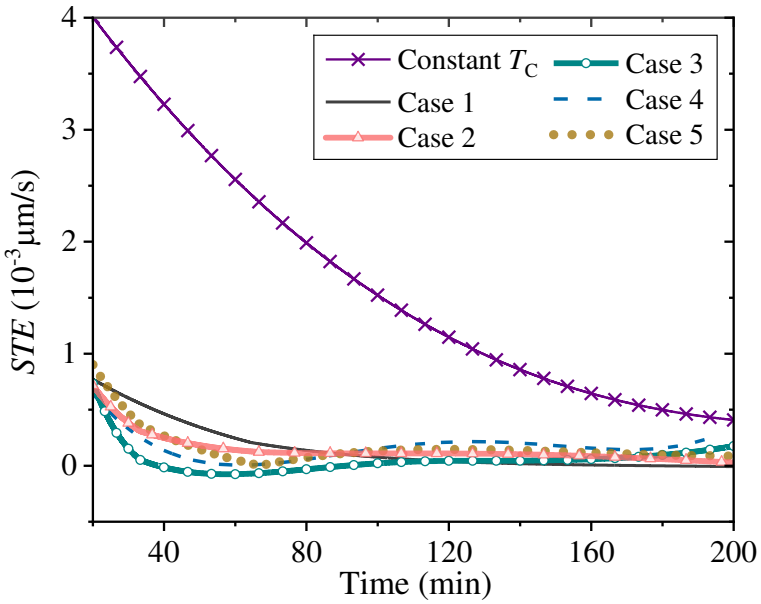

Fig. 9 STE variations of the closed-loop thermal control and constant temperature cooling

The thermal error is considered as stable when absolute value of STE becomes less than 0.25×10^{-3}μm/s, which is the thermal equilibrium state. For the presented five cases of thermal error feedback control, the STE curves respectively become less than 0.25×10^{-3}μm/s after 51, 31, 45, 49 and 43 minutes. The thermal equilibrium state respectively maintained stable for 249, 169, 205, 151 and 157 minutes. The EVR (Thermal Error Variation Rage) are respectively 1.513μm, 1.487μm, 1.637μm, 1.482μm and 1.508μm.

The spindle can hardly reach thermal equilibrium state with constant temperature cooling. If we relax the judging criteria for the thermal error equilibrium-state to a STE value of 0.5×10^{-3}μm/s, comparing with that of constant temperature cooling, the time for reaching the equilibrium-state is respectively advanced by 78.3%, 86.7%, 86.9%, 83.8% and 87.8% in the five cases of thermal error feedback control.

5.4 Model performance analysis

Five experiments are conducted with the RFR model, for which the maximum T_C deviation at any time point is pre-estimated to be 0.93℃. For the five cases of feedback control based active cooling experiments, the online thermal error estimations are compared with the actual thermal error measurements (Fig. 10). Time interval for the model to output an estimation is 180 seconds, which equals the time interval that the online temperature measurements are processed to mean moving average.

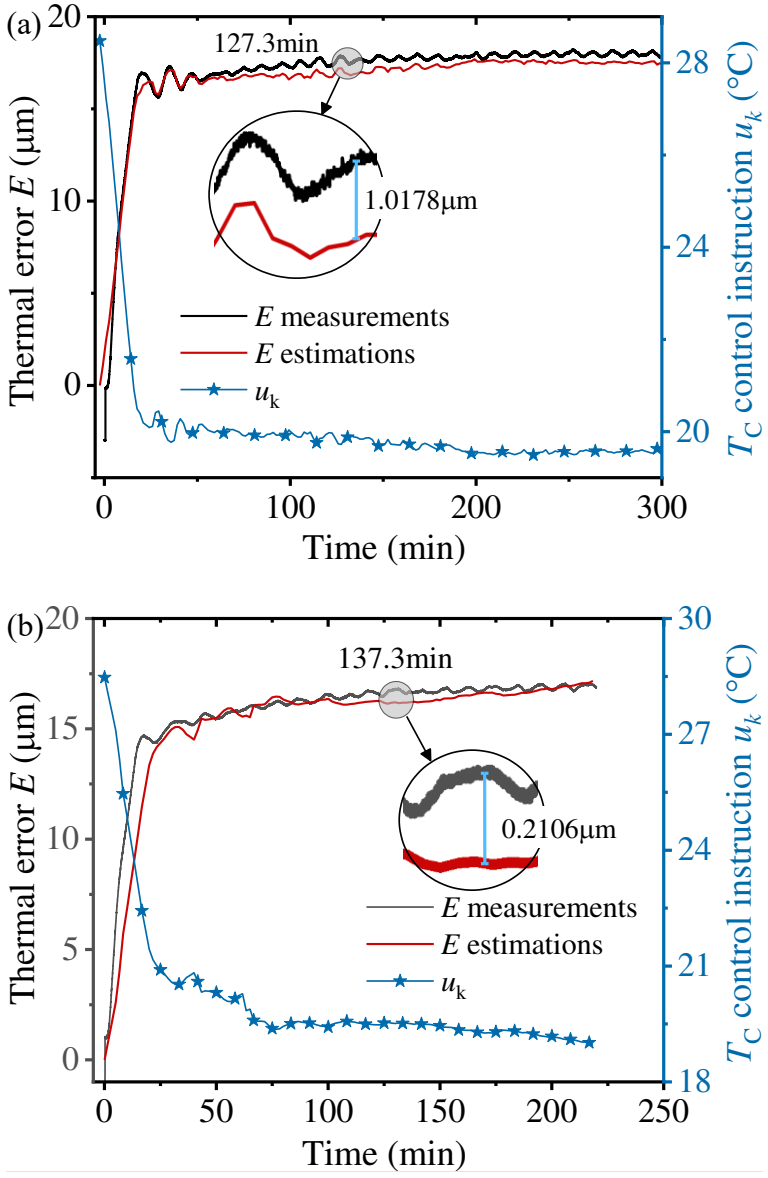

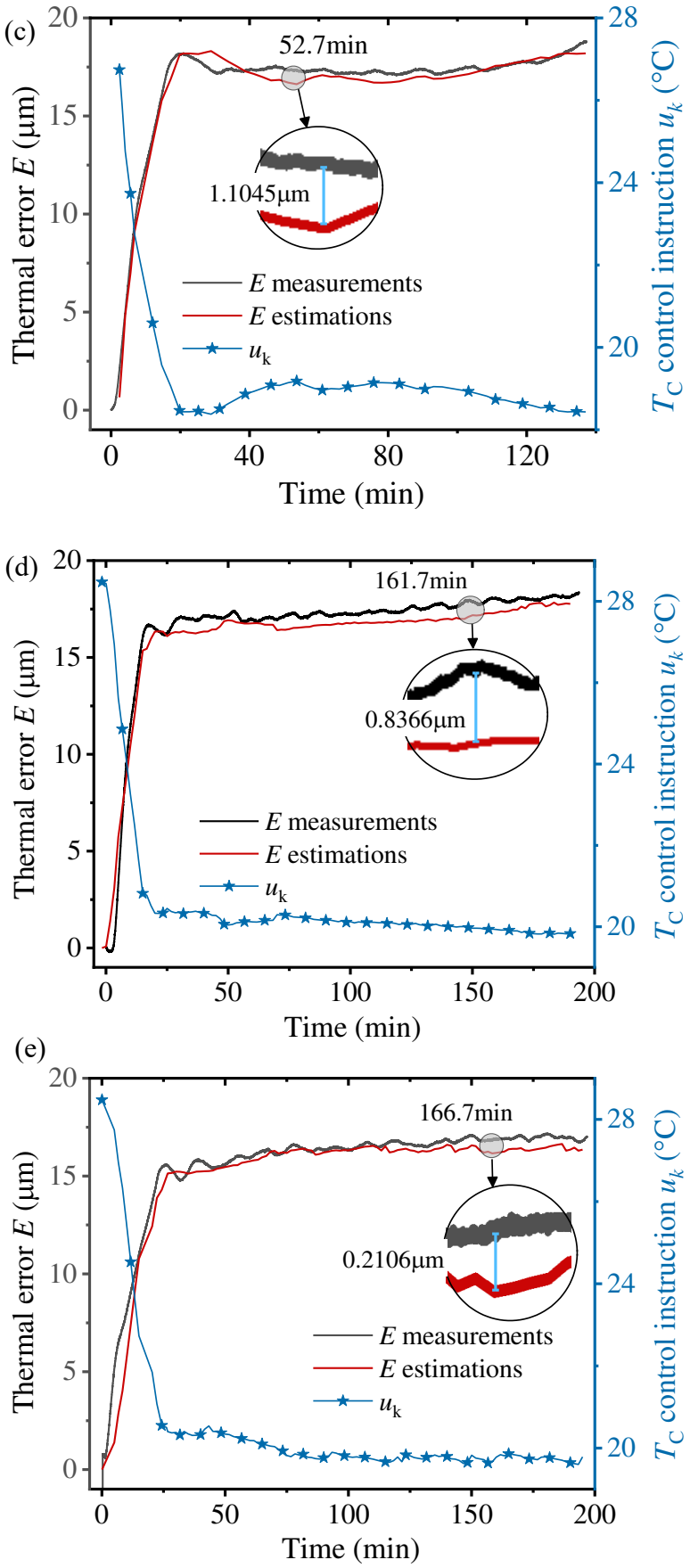

Fig. 10 Comparisons between the estimated and measured thermal error E: (a) Case1; (b) Case2; (c) Case3; (d) Case4; (e) Case5.

Case 1 and 2 are conducted under the rotation speed condition of 3000rpm which is similar as the experiments for collecting training data. Case 3, 4 and 5 are conducted under the unseen work conditions of varying rotation speed. In the thermal equilibrium state, the maximum differences (estimation residual) between measured and estimated E(by summing ΔE) are respectively 1.0178(127.3min), 0.2106(161.7min), 1.1045(52.7min), 0.2079 (166.7min) and 0.8366 (137.3min). Above large E residuals are formed by accumulation of the ΔE estimation residuals, which is the systematic error of feedback. As a result, spindle thermal error kept increasing slowly in Case 1~5 in the thermal equilibrium state, but are within the expected variation range all the time.

If we exclude the observations of the pre-heating stage and consider only those in the equilibrium-state, the goodness of fit of the model will reflect whether reliable feedback is outputted for the thermal error feedback control, so that the thermal error will be stabilized in long-term. Three evaluation criterions, the *MSE*, the determination coefficient R, and the accuracy η are introduced to assess the model performance in the thermal error feedback control process:

$$MSE = \frac{1}{n}\sum_{i=1}^{n}(y_i - \hat{y}_i)^2 \tag{33}$$

$$R = 1 - \frac{\sum_{i=1}^{n}(y_i - \hat{y}_i)^2}{\sum_{i=1}^{n}(y_i - \bar{y}_i)^2} \tag{34}$$

$$\eta = 1 - \frac{\sum_{i=1}^{n}|y_i - \hat{y}_i|}{\sum_{i=1}^{n}|y_i|} \tag{35}$$

and the model performance evaluation results are presented in Table 5. The *MSE* value are smaller than 0.5159; the predicting accuracies (η) are all more than 9.494%; the determination parameters (R) are more than 0.9640.

Table 5. Model performance evaluation for the equilibrium-stage

	Case 1	Case 2	Case 3	Case 4	Case 5
MSE	0.2897	0.4105	0.3499	0.4451	0.5159
R	0.9640	0.9656	0.9748	0.9663	0.9742
η	0.9736	0.9650	0.9703	0.9791	0.9494

6. Conclusion

A novel thermal error feedback control based active cooling strategy is proposed for stabilizing the thermal error of a precision mechanical spindle in long term. Independence of the spindle thermal data is tested, and a V-C dimension based approach is presented to estimate the generalization error bound of the model for outputting feedbacks, so reliability of the thermal error feedback control processes can be pre-estimated. Core conclusions of this study are as follows:

(1) Spindle thermal data which include temperature and thermal error are obviously dependent. The multivariate portmanteau statistic based independent testing is performed on the thermal variation data and indicated that only slight violation to the independent hypothesis. As a result, it is reasonable to perform independence hypothesis based algorithms on the spindle thermal variation data.

(2) Feedback inaccuracy is due to the insufficient generalization performance of the spindle thermal error model. A V-C dimension based approach is proposed to estimate the generalization error bounds of the thermal error regression models. Thus, the model which is most likely to give acceptable performance can be selected, and the feedback inaccuracy can be bounded. It can be estimated that the maximum deviation of T_C is no more than 0.93℃ at any timepoint if the RFR model is employed, so the thermal error fluctuation range is assumed to be acceptable.

(3) STE are quantitatively evaluated using discrete derivative of the fitted smooth curves, and the spindle is regarded as equilibrium-state when STE keeps smaller than a threshold. In the five cases of thermal feedback control, the STE curves becomes under 0.25×10^{-3}μm/s in less than 51 minutes, cooling with constant coolant temperature cannot achieve such stability. For the relaxed thermal equilibrium-state criteria of the STE value of 0.5×10^{-3}μm/s, compared with the constant T_C cooling, the thermal error

feedback control based active cooling method advances the time for reaching the equilibrium-state by 78.3%~87.8% in the five cases. Moreover, in the equilibrium-state of the thermal error feedback control processes, the thermal error variation range are kept to 1.482~1.637μm for more than 150 minutes.

For further research, this method should be extended for various kinds of spindles in precision machine tools under diverse work conditions, and the pre-heating time should be shortened.

Acknowledgments

The author(s) disclosed receipt of the following financial support for the research, authorship, and/or publication of this article: Natural Science Basic Research Program of Shaanxi (2021JQ-475), Start-up fund of Xi'an University of Technology (451120007), the Science and Technology Major Project of Shaanxi Province (No. 2018ZDZX01-02-01), and the Shandong Tai Shan industrial leader talent project (No. 2017TSCYCX-24).

Author contribution Mohan Lei: Conceptualization, Methodology, Writing- Original draft preparation. Feng Gao: Investigation, Validation. Yan Li: Software. Ping Xia: Software, Writing- Reviewing and Editing. Mengchao Wang: Validation. Jun Yang: Supervision.

Availability of data and material All experimental data of this study are available.

Code availability Not applicable.

Declarations

Ethics approval Not applicable.

Consent to participate All the authors involved have agreed to participate.

Consent for publication All the authors involved have agreed to publish this work.

Conflict of interest The authors declare no competing interests.

References

[1] L. Weng, W. Gao, D. Zhang, et al. Analytical modelling method for thermal balancing design of machine tool structural components. International Journal of

Machine Tools and Manufacture, 2021: 103715.
[2] TJ. Li, CY. Zhao, YM. Zhang. Real-time thermal error prediction model for CNC lathes using a new one-dimension lumped capacity method[J]. The International Journal of Advanced Manufacturing Technology, 2021. 117(1-2):1-12.
[3] J. Liu, C. Ma, et al. Thermal-structure interaction characteristics of a high-speed spindle- bearing system - ScienceDirect. International Journal of Machine Tools and Manufacture, 2019. 137(1-2): 42-57.
[4] Y. Yang, ZC. Du, et al. Real-time thermal modelling approach of a machine tool spindle based on bond graph method. The International Journal of Advanced Manufacturing Technology, 2021. 113:99-115.
[5] H. Cao, XW. Zhang, XF. Chen, et al., The concept and progress of intelligent spindles: A review. International Journal of Machine Tools and Manufacture, 2017, 112:21-52.
[6] Z. Li, G. Li, K. Xu, et al. Temperature-sensitive point selection and thermal error modeling of spindle based on synthetical temperature information[J]. The International Journal of Advanced Manufacturing Technology, 2021, 113(3-4):1-15.
[7] Z. Zou, W. Yan, W. Ma, et al. Development of thermal error mapping model for the dry gear hobbing machine based on CNN-DAE integrated structure and its application[J]. The International Journal of Advanced Manufacturing Technology, 2021, 113(7):2343-2354.
[8] T. Liu, WG. Gao, YL. Tian, et al. A differentiated multi-loops bath recirculation system for precision machine tools. Applied Thermal Engineering, 2015. 76: 54-63.
[9] WF. Chang, WG. Gao, DW. Zhang, et al. Power matching based dissipation strategy onto spindle heat generations. Applied Thermal Engineering, 2017. 113: 499-507.
[10] SN. Grama, A. Mathur, AN Badhe. A model-based cooling strategy for motorized spindle to reduce thermal errors. International Journal of Machine Tools and Manufacture, 2018. 132: 3-16.
[11] ZJ. Ge, XH. Ding. Design of thermal error control system for high-speed motorized spindle based on thermal contraction of CFRP. International Journal of Machine Tools and Manufacture, 2018. 125: 99-111.
[12] MH. Lei, GD. Jiang, L. Zhao, et al. Thermal error controlling for the spindle in a precision boring machine with external cooling across coated joints. Proceedings of the Institution of Mechanical Engineers, Part C-Journal of Mechanical Engineering Science. 2019, 234(2): 658-675.
[13] K. Liu, et al. Modeling and compensation for spindle's radial thermal drift error on a vertical machining center. International Journal of Machine Tools and Manufacture, 2016. 105: 58-67.
[14] J. Yang, H. Shi, B. Feng, et al., Thermal error modeling and compensation for a high-speed motorized spindle. The International Journal of Advanced Manufacturing Technology, 2015. 77(5): 1005-1017.
[15] E. Miao, Y. Liu, H. Liu, et al., Study on the effects of changes in temperature-

sensitive points on thermal error compensation model for CNC machine tool. International Journal of Machine Tools & Manufacture, 2015, 97: 50-59.
[16] M. Mpoudeu, B. Clarke. Model Selection via the VC-Dimension. 2018.
[17] PB. Zhang, ZX. Yang. A Novel AdaBoost Framework With Robust Threshold and Structural Optimization. IEEE Transactions on Cybernetics, 2016, 48(1): 1-13.
[18] C. Ma, J. Yang, et al., Simulation and experimental study on the thermally induced deformations of high-speed spindle system. Applied Thermal Engineering, 2015. 86: 251-268.
[19] MH. Lei, GD. Jiang, J. Yang, et al. Improvement of the regression model for spindle thermal elongation by a Boosting-based outliers detection approach. The International Journal of Advanced Manufacturing Technology, 2018. 99(5): 1389-1403.
[20] E. Mahdi, AI. Mcleod. Improved multivariate portmanteau test[J]. Journal of Time Series Analysis, 2012, 33(2): 211-222.
[21] J. Hosking. The Multivariate Portmanteau Statistic. Publications of the American Statistical Association, 1980, 75(371): 602-608.
[22] MH. Lei, GD. Jiang, J. Yang, et al., Thermal error modeling with dirty and small training sample for the motorized spindle of a precision boring machine. The International Journal of Advanced Manufacturing Technology, 2017. 93(1-4): 571–586.
[23] EM. Miao, Y. Liu, H. Liu, et al. Study on the effects of changes in temperature-sensitive points on thermal error compensation model for CNC machine tool[J]. International Journal of Machine Tools and Manufacture, 2015.
[24] D. Basak, P. Srimanta, DC. Patranbis. Support Vector Regression[J]. Neural information processing letters & reviews, 2007, 11(10):203-224.
[25] V. Vapnik. The nature of statistical learning theory. Springer science & business media, 2013.
[26] S. Xu, X. An, X. Qiao, et al. Multi-output least-squares support vector regression machines[J]. Pattern Recognition Letters, 2013, 34(9):1078-1084.
[27] V. Cherkassky, Y. Ma. Practical selection of SVM parameters and noise estimation for SVM regression. Neural Networks, 2004, 17(1): 113-126.
[28] SN. Sivanandam, SN. Deepa. Introduction to Genetic Algorithms[M]. Springer Berlin Heidelberg, 2008.
[29] L. Breiman. Random Forests. Machine Learning, 2001, 45(1): 5-32.
[30] G. Zhang, Y. Lu. Bias-corrected random forests in regression. Journal of Applied Statistics, 2012, 39(1): 151-160.
[31] S. Gey, E. Nédélec. Model selection for CART regression trees. IEEE Transactions on Information Theory, 2005, 51(2): 658-670.
[32] GF. Ziarh, S. Shahid, TB. Ismail, et al. Correcting bias of satellite rainfall data using physical empirical model[J]. Atmospheric Research, 2020, 251:105430.
[33] MT. Mpoudeu. Use of Vapnik-Chervonenkis Dimension in Model Selection. 2017.